Toward Massive Ray-Based Simulations of mmWave Small Cells on Open Urban Maps

Dmitrii Solomitckii, Margarita Gapeyenko, Sebastian S. Szyszkowicz, *Member, IEEE*,
Sergey Andreev, *Member, IEEE*, Halim Yanikomeroglu, *Fellow, IEEE*,
and Yevgeni Koucheryavy, *Senior Member, IEEE*

Abstract—**High-rate access in outdoor urban areas using extremely high frequency (EHF) bands, known as *millimeter-wave* (mmWave) spectrum, requires a dense deployment of wireless small cells in order to provide continuous coverage to serve bandwidth-hungry users. At the same time, to be able to collect a sufficient amount of data for constructing detailed EHF propagation models, a considerable number of various landscape maps across different scenarios have to be considered. This letter develops a *shoot-and-bounce ray (SBR)*-based methodology capable of characterizing the mmWave propagation in *urban outdoor* conditions. In particular, our methodology aims to capture a large number of small cells within accurate, *real city maps* and then to utilize an algorithm of automatic transmitter placement. Hence, our contribution is to provide a suitable tool that is able to handle *massive ray-based simulations* within a reasonable time frame. In particular, we demonstrate and verify that a shift from simulating three-dimensional (3-D) to evaluating 2-D environments significantly reduces computation time while only slightly decreasing the simulation accuracy.**

Index Terms—**Dense urban deployments, massive ray-based simulations, millimeter-wave (mmWave) small cells, shoot-and-bounce ray (SBR) modeler.**

I. Introduction and Background

THE increase in traffic demand together with the growing needs for higher user data rates and lower latencies require the introduction of innovative concepts as part of the fifth-generation mobile networks. The extremely high frequency (EHF) band is a promising candidate to support many key requirements of next-generation wireless communication systems. Making use of larger bandwidths, the millimeter-wave (mmWave) spectrum available in the EHF band is expected to enable several Gb/s of data rate [1].

In addition to its benefits, mmWave system operation also poses unprecedented challenges. One of these is completely *new channel characterization* that is not applicable in lower frequency bands. Due to the very different nature of the mmWave spectrum, one of the potential difficulties is considerable *blockage* caused by smaller objects [2], [3]. In addition, diffuse scattering needs to be accounted for in mmWave systems. All of the above brings the need to comprehensively analyze the propagation characteristics that are not similar to those in lower frequency bands.

For the above reasons, multiple studies focused on obtaining statistics desirable for channel characterization through real measurements or simulations. Today, deterministic site-specific tools, such as three-dimensional (3-D) ray tracing (RT) and ray launching (RL), remain widely popular to simulate wireless propagation in indoor and outdoor environments alike. Even though there are numerous studies describing the RT tools in order to quantify the channel behavior, the main limitation of the past works is in their small study regions. Also, although various techniques were employed to speed up the simulations [4], the resultant speed may still be insufficient to capture larger city maps with many transceivers. A propagation study over a vast urban area has the advantage of being more representative of the entire city, without potential artifacts arising from investigating a particular location. Since placing many transmitters (TXs) by hand is impractical, an algorithm needs to be developed for this purpose, e.g., [5].

In this letter, we outline a methodology that can statistically describe wireless channel properties based on the deterministic data obtained from a *large number of real maps*. The obtained data can be used to gain a deeper understanding of the mmWave propagation properties in a typical city. Moreover, our methodology is also capable of resolving the main challenges that arise from obtaining a large number of statistical inputs needed for channel modeling. As small cells in the EHF band are expected to offer shorter coverage ranges compared to those in the lower frequency bands [1], [3], it is important to have more TXs for uninterrupted coverage.

The rest of this letter is organized as follows. The proposed methodology and the map preparation technique are provided in Section II. In Section III, the deterministic site-specific simulation tool is described. The verification of the proposed methodology is discussed in Section IV. The conclusions and future work are given in Section V.
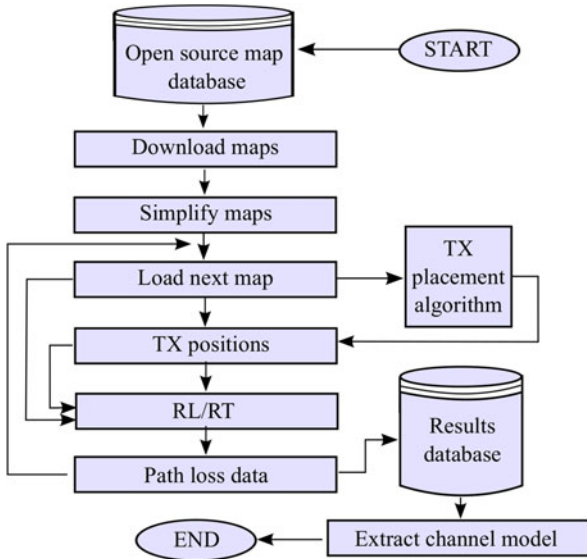
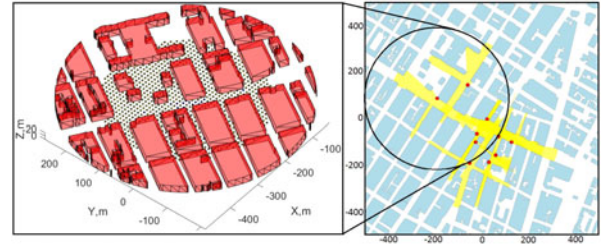Fig. 1. Flowchart of the proposed methodology.

Fig. 2. Sample map of Manhattan Island (right image), centered at (73.99 W, 40.73 N) with ten TXs placed on wall sides, with reasonable LoS coverage (shown in yellow). Our simulation campaign comprises nine of such maps. Each map is divided into smaller areas (left image) with TX in the center.

TABLE I
OUR DEPLOYMENT PARAMETERS

Parameter	Value
Center of area of interest	73.99 W 40.73 N
Total area of interest	2000 m × 2000 m
Average coverage by buildings	47 %
Total number of maps	3 × 3
Individual map size	1000 m × 1000 m
Overlap of adjacent maps	by 500 m
Inner area size with placed TXs	600 m × 600 m
Number of TXs	10 per map, 90 in total
TX height	10 m
RX locations	outdoor, RX-grid
RX height	1.5 m
Number of RXs	1250 per inner area
Building material	concrete ($\epsilon_r = 5.31$, $\sigma_r = 0.484$)
Antennas	isotropic radiator

II. PROPOSED METHODOLOGY

In order to simulate a significant number of maps, it is important to have the key components including a large database of maps, an algorithm for the automatic placement of TXs on a map, and a fast ray-based simulation tool. The flowchart of the proposed methodology is shown in Fig. 1. The core idea is based on generating multiple maps, automatically producing "good" TX locations for each one, and uploading the maps into a ray-based simulator one by one. As the maps are processed, the statistical data can be used to derive accurate channel models for large urban areas.

The real maps of 2-D buildings can be extracted from the OpenStreetMap project (or similar) as described in [6] and [5], where each building is represented by a simple polygon. The adjacent buildings are merged together and the inside areas (e.g., courtyards) are removed. The algorithm that searches for the appropriate TX locations on the facades of the buildings is described in [5]; it identifies TX positions that lead to the adequate line-of-sight (LoS) area within a certain distance (200 m based on current mmWave research [1], [3], [5]).

In this letter, we focus on the verification of our methodology by considering a typical urban area: Manhattan Island. However, the choice of the urban layout is not limited to our example, and we plan to use other areas in our future studies. The Manhattan grid is used as a reference use case in many existing standards, such as [7], and one can therefore reasonably compare these results to other work. In Section IV, we contrast the overall accuracy of our methodology against the models proposed by 3GPP [7] for the urban microcell.

According to this methodology, we study nine square maps, each with ten deployed TXs (see Fig. 2), which are chosen randomly from the candidate points generated by the algorithm in [5]. The middle map of our simulation campaign is shown in the right side of Fig. 2. Every map is of size 1000 × 1000 m², but only the inner 600 × 600-m² square is considered for the TX locations to avoid edge effects. Therefore, different maps

may overlap partially to reuse the building-related data. Our simulation scenario is summarized in Table I.

III. SIMPLIFIED RAY-BASED SIMULATOR

A. 3-D to 2-D Conversion

To perform the targeted massive simulations and extract a significant amount of statistical data, one of the key components is to have a ray-based simulation tool that is fast enough. For this purpose, we reduce the space dimensionality of our ray propagation simulator as well as that of the maps from true 3-D to 2-D. This transformation becomes possible because mmWave access points are expected to be located significantly below rooftop and the rooftop diffraction can be ignored. Based on this model, wave propagation occurs in a 2-D xy-plane, where multiple TXs and receivers (RXs) are positioned at the same height. In case the TX height differs from that of the RX, the xy-plane is transformed (typically, rotated around x- or y-axis), so that both antennas belong to it and the propagation occurs in the modified plane. However, a 2-D implementation—due to the absence of the third dimension (z-axis)—has a limitation in that it does not straightforwardly take into account the role of the ground-reflected beams. Hence, we added extra beams reflected from the ground. This was done utilizing the elements of the so-called two-ray model [8], which does not require any additional geometric simulations, which are very time-consuming. The above improvements are valid if it is assumed that all of the building walls are orthogonal to the ground plane, which is
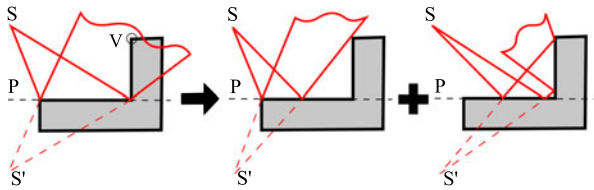
Fig. 3. Decomposition of the first beam (left image) from source S impinging on the internal edge of plane P that produces $N + 1$ secondary beams (center and right images), where N is number of occluded vertices V in main beam.

common for urban scenarios. If some of these requirements are not met, then a true 3-D ray-based simulator must be used.

B. Utilized Shoot-and-Bounce Ray (SBR) Launching Method

A key element in accelerating ray-based simulations is the image-based SBR method, whose basic principles were described in [9]–[11]. Accordingly, the geometrical engine searches for paths between mutually visible objects (walls, edges, antennas, etc.) using the image method. Then, the physical engine calculates a number of phenomena, such as reflection, transmission, and diffraction, by following the geometrical optics principles and employing the uniform theory of diffraction. Our hybrid technique integrates the image-based RT and brute-force RL, removing all the inherent limitations of both models. The main advantage is in lower simulation time with respect to the canonical RT and RL, which plays a crucial role in massive simulations.

An enhanced SBR-based geometrical engine was designed, which is composed of two stages: 1) construction of a hierarchical visibility tree, and 2) search for all the unique paths between the TX and the RX. The first tree identifies all the mutually visible objects, whereas the second tree builds a visibility abstraction for the specific TX–RX pairs based on the first tree data. Such a hierarchical approach offers higher efficiency when hundreds of TXs within a complex scenario need to be simulated, but does not provide advantages in simpler scenarios. Once constructed, the first visibility tree for a single scenario may be used repeatedly by all the antennas, which unlocks a speed gain.

Instead of using thousands of infinitely thin lines as conventional RL does, the SBR operates with fewer beams, modeled by triangles. Such an approach reduces the amount of processing, but requires smart algorithms for beam propagation and interaction modeling. One of the key tasks here is beam partitioning, which occurs when the beam impinges on a wall. Our implementation is based on a search of occluded vertices V within a triangle to perform the beam splitting, as shown in Fig. 3. The algorithm at its second stage builds TX-to-RX paths through the intermediate projections on objects that are included into the visibility tree from the first stage.

IV. SIMULATION RESULTS AND DISCUSSION

In this section, we present our 3-D and 2-D simulation results for multiple outdoor urban maps, using the true 3-D SBR, the true 2-D SBR (propagation in a plane, without the ground-bouncing beams), and the improved 2-D SBR (with ground-bouncing beams). The TX positions are automatically planned in

TABLE II
COMPARISON TO 3GPP PARAMETERS

Parameter	Improved 2-D SBR	3GPP
Rician K-factor	$\mu = 13.7$	$\mu = 9, \sigma = 5$
$\log_{10}$ (delay spread, s)	LoS: $\mu = -7.3$	LoS: $\mu = -7.49, \sigma = 0.38$
	nLoS: $\mu = -6.8$	nLoS: $\mu = -7.18, \sigma = 0.51$
$\log_{10}$ (AoA spread, °)	LoS: $\mu = 1.5$	LoS: $\mu = 1.61, \sigma = 0.30$
	nLoS: $\mu = 2.1$	nLoS: $\mu = 1.69, \sigma = 0.37$
$\log_{10}$ (AoD spread, °)	LoS: $\mu = 1.3$	LoS: $\mu = 1.13, \sigma = 0.41$
	nLoS: $\mu = 1.4$	nLoS: $\mu = 1.19, \sigma = 0.49$

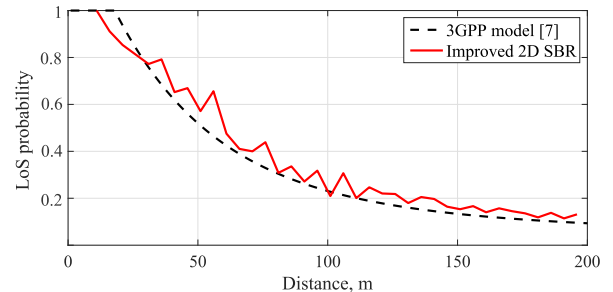μ: mean parameter value; σ: standard deviation of parameter value

Fig. 4. Comparison of LoS probability: Improved 2-D SBR with ground-bouncing rays versus 3GPP model in [7].

the central $600 \times 600\text{-m}^2$ area, while all the RXs are distributed across the outdoor locations. All of the antennas are isotropic and vertically polarized without any mismatch; their radiated power is 25 dBm, and the frequency is 28 GHz. The material properties, such as the dielectric permittivity and conductivity, are taken from [12].

To verify the accuracy of our improved 2-D SBR, we compare its output to the key channel parameters considered by 3GPP: the K-factor, the delay spread, the angle of arrival (AoA) spread, the angle of departure (AoD) spread, and the LoS probability. This is a crucial step since all the wireless channel related metrics will be of importance in other environments. Hence, they must first be validated by our study. To make a connection between the 3GPP's stochastic/empirical models and the deterministic results, massive simulations need to be performed to collect as many statistics as possible. Finally, we average each of the above parameters, producing the mean value as per 3GPP procedures. The results are summarized in Table II.

The LoS probability and the path loss (PL) are compared in Figs. 4 and 5, respectively. Being a purely geometrical property, the LoS probability verifies our geometrical engine and is calculated in two steps: 1) connect each of the TX-RX pairs by a line, and 2) check for the intersections of the line with any surrounding objects.

It can be observed that the simulated mean values (μ) of channel properties in Table II and Figs. 4 and 5 are close to the ones proposed by 3GPP in [7]. However, the properties shown in Table II for some of the RXs in non-LoS (nLoS) conditions are outside of the standard deviation limit (σ) considered by 3GPP for the bands above 6 GHz. The reason for this is the restrictions of the 3GPP environment, which assumes the idealized Manhattan grid. While we also select Manhattan city maps for our simulations, most real layouts still have irregular Manhattan
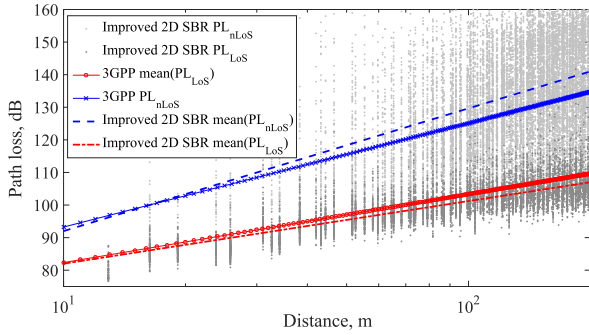
Fig. 5. Comparison of PL: Improved 2-D SBR versus 3GPP model [7]. Dark points are PL from TX to LoS RXs; light points are PL to nLoS RXs.
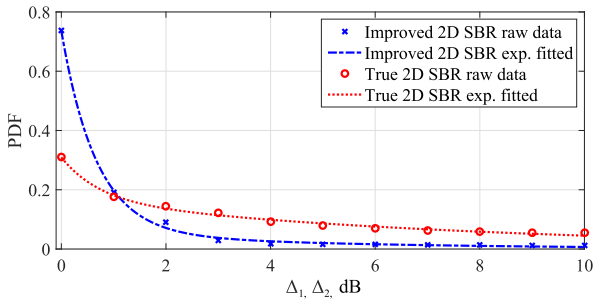

Fig. 6. Total received power difference: Improved 2-D SBR versus true 2-D SBR.

grid topology (see Fig. 2). Hence, real beams may propagate over much longer/shorter distances compared to similiar paths in the canonical Manhattan grid topology.

Another important aspect is the role and the importance of the ground-bouncing rays for the total received power calculations. Therefore, we compare the true 3-D SBR, the true 2-D SBR, and the improved 2-D SBR (with additional ground-bouncing rays) in terms of the simulation time and accuracy of the total received power estimation. The results indicate that the true 2-D SBR and the improved 2-D SBR are approximately $15\times$ faster compared to the true 3-D SBR since the amount of processing is lower. The accuracy of the total received power is given as the distribution of difference between the true and the improved 2-D SBR versus the 3-D SBR as follows:

$$\Delta_1 = |P_{\text{3DSBR}_{\text{true}}}^{\text{tot}} - P_{\text{2DSBR}_{\text{true}}}^{\text{tot}}| \tag{1}$$

$$\Delta_2 = |P_{\text{3DSBR}_{\text{true}}}^{\text{tot}} - P_{\text{2DSBR}_{\text{improved}}}^{\text{tot}}|. \tag{2}$$

Hence, we characterize the distribution of differences Δ_1 and Δ_2 among RXs in true and improved 2-D SBR, respectively (shown in Fig. 6). Note that the results obtained with the improved 2-D SBR are closer to 3-D SBR than those produced with true 2-D SBR, and the additional ground-bouncing beams really make a difference. The maximum observed Δ_2 is about 5 dB (only for 1 % of all RXs), and almost 80 % of the RXs have a total received power similar to the true 3-D SBR.

V. CONCLUSION AND FUTURE WORK

The different propagation effects of the EHF band together with the smaller cell coverage ranges require a novel modeling approach that is capable of supporting extensive studies of the mmWave channel. Along these lines, the main focus of this letter is massive simulations for a large number of mmWave small cells located on multiple maps of a real city. While existing RL and RT studies focused mainly on simulating a single map of a simplified deployment, our methodology extends the limits of deterministic modeling toward statistical studies. Results produced by our approach might be used to develop new analytical models as well as to complement the existing standards, such as COST, WINNER, 3GPP, ITU-R, and others. We propose a novel 2-D SBR-based methodology that is able to collect the mmWave channel statistics from several realistic city maps in a reasonable time. The computation time for our 2-D SBR is about $15\times$ shorter than that for the true 3-D SBR. Furthermore, adding ground-bouncing rays to the 2-D SBR may significantly improve the total accuracy while maintaining efficient simulation times.

Finally, we compare the output of the 2-D SBR against the existing 3GPP models and confirm that the proposed methodology offers an accurate approach for collecting statistical data in the environment of interest. One limitation of our improved 2-D SBR is in that it can only work in the deployments where all of the walls are strictly perpendicular to the ground and the antennas are positioned significantly below rooftops. As our next step, we aim to validate our 2-D SBR simulator against mmWave measurements. In addition, we may need to design methods that support beamforming antenna arrays, which will become an important consideration in the future mmWave systems.

REFERENCES

[1] J. G. Andrews *et al.*, "What will 5G be?" *IEEE J. Sel. Areas Commun.*, vol. 32, no. 6, pp. 1065–1082, Jun. 2014.

[2] M. Gapeyenko *et al.*, "Analysis of human-body blockage in urban millimeter-wave cellular communications," in *Proc. IEEE Int. Conf. Commun.*, May 2016, pp. 1–7.

[3] S. Rangan, T. S. Rappaport, and E. Erkip, "Millimeter-wave cellular wireless networks: Potentials and challenges," *Proc. IEEE*, vol. 102, no. 3, pp. 366–385, Mar. 2014.

[4] G. Durgin, N. Patwari, and T. S. Rappaport, "An advanced 3D ray launching method for wireless propagation prediction," in *Proc. IEEE Veh. Technol. Conf.*, May 1997, vol. 2, pp. 785–789.

[5] S. S. Szyszkowicz, A. Lou, and H. Yanikomeroglu, "Automated placement of individual millimeter-wave wall-mounted base stations for line-of-sight coverage of outdoor urban areas," *IEEE Wireless Commun. Lett.*, vol. 5, no. 3, pp. 316–319, Jun. 2016.

[6] M. Mirahsan, R. Schoenen, S. S. Szyszkowicz, and H. Yanikomeroglu, "Measuring the spatial heterogeneity of outdoor users in wireless cellular networks based on open urban maps," in *Proc. IEEE Int. Conf. Commun.*, Jun. 2015, pp. 2834–2838.

[7] *Channel Model for Frequency Spectrum above 6 GHz (Release 14)*, 3GPP TR 38.900 V2.0.0, Jun. 2016.

[8] R. Aquino-Santos, *Wireless Technologies in Vehicular Ad Hoc Networks: Present and Future Challenges*, A. Edwards and V. Rangel Licea, Eds. Hershey, PA, USA: IGI Global, 2012.

[9] H. S. Sato and K. Otoi, "Electromagnetic wave propagation estimation by 3-D SBR method," in *Proc. Int. Conf. Electromagn. Adv. Appl.*, Sep. 2007, pp. 129–132.

[10] S. H. Chen, "An SBR/image approach for radio wave propagation in indoor environments with metallic furniture," *IEEE Trans. Antennas Propag.*, vol. 45, no. 1, pp. 98–106, Jan. 1997.

[11] S. Chen and S. K. Jeng, "SBR image approach for radio propagation in tunnels with and without traffic," *IEEE Trans. Veh. Technol.*, vol. 45, no. 3, pp. 570–578, Sep. 1996.

[12] *Effects of Building Materials and Structures on Radiowave Propagation Above About 100 MHz*, ITU-R P.2040-1, Jul. 2015.